Mitochondria regulate intestinal stem cell proliferation and epithelial homeostasis through FOXO

Fan Zhang, Mehdi Pirooznia, and Hong Xu*
National Heart, Lung, and Blood Institute, National Institutes of Health, Bethesda, MD 20892

ABSTRACT **A metabolic transition from glycolysis to oxidative phosphorylation is often associated with differentiation of many types of stem cells. However, the link between mitochondrial respiration and stem cells' behavior is not fully understood. We genetically disrupted electron transport chain (ETC) complexes in the intestinal stem cells (ISCs) of *Drosophila*. We found that ISCs carrying impaired ETC proliferated much more slowly than normal and produced very few enteroblasts, which failed to further differentiate into enterocytes. One of the main impediments to ISC proliferation and lineage specification appeared to be abnormally elevated forkhead box O (FOXO) signaling in the ETC-deficient ISCs, as genetically suppressing the signaling pathway partially restored the number of enterocytes. Contrary to common belief, reactive oxygen species (ROS) accumulation did not appear to mediate the ETC mutant phenotype. Our results demonstrate that mitochondrial respiration is essential for *Drosophila* ISC proliferation and lineage specification in vivo and acts at least partially by repressing endogenous FOXO signaling.**

Monitoring Editor
Thomas Fox
Cornell University

Received: Oct 4, 2019
Revised: Apr 20, 2020
Accepted: Apr 28, 2020

INTRODUCTION

Eukaryotes utilize either glycolysis or oxidative phosphorylation (OXPHOS) to extract energy from food and store it as the high-energy ATP molecule. Unlike glycolysis, which partially metabolizes glucose to pyruvate, OXPHOS completely oxidizes glucose to CO_2 and is much more efficient in harnessing energy (Wallace, 2012). OXPHOS is carried out by the electron transport chain (ETC) complexes and mitochondrial ATP synthase located on the mitochondrial inner membrane. Mitochondria are thought to evolve from endosymbiotic bacteria. Over the course of evolution, most mitochondrial genes have migrated to the nucleus, whereas core ETC subunits still remain on the mitochondrial genome (mtDNA) (Wallace, 2012). To accommodate different metabolic profiles and energy demands, cells in different tissues and developmental stages modulate the amount of mtDNA they contain and its expression level (Moraes, 2001). The dynamic regulation of mitochondrial activity is particularly evident during stem cell differentiation. Many types of stem cells favor glycolysis even in the presence of oxygen, a phenomenon termed as "aerobic glycolysis" (Vander Heiden *et al.*, 2009; Rafalski *et al.*, 2012; Lisowski *et al.*, 2018), but undergo a metabolic transition during differentiation (Folmes *et al.*, 2012; Zheng, Boyer, *et al.*, 2016), increasing mitochondrial mass (Cho *et al.*, 2006; Prigione *et al.*, 2010; Zhang, Marsboom, *et al.*, 2013), mtDNA copy number (Cho *et al.*, 2006; Facucho-Oliveira *et al.*, 2007; Wanet *et al.*, 2014), and respiratory activity (von Heimburg *et al.*, 2005; Zhang, Marsboom, *et al.*, 2013; Wanet *et al.*, 2014). Pharmacological or genetic disruptions of ETC complexes often block stem cell differentiation (Chung *et al.*, 2007; Mandal *et al.*, 2011) or interfere with lineage specification (Inoue *et al.*, 2010; Cherry, Gagne. *et al.*, 2013; Diaz-Castro, Pardal, *et al.*, 2015), indicating an involvement of mitochondrial respiration in regulating stem cells' activity. However, it is largely unknown how ETC complexes interact with the cellular signaling pathways to influence stem cell behavior.

The *Drosophila* adult midgut is a well-established model to study stem cell behavior. Intestinal stem cells (ISCs) have been found

This article was published online ahead of print in MBoC in Press (http://www.molbiolcell.org/cgi/doi/10.1091/mbc.E19-10-0560) on May 6, 2020.

*Address correspondence to: Hong Xu (xuh5@nhlbi.nih.gov).

Abbreviations used: 4EBP, 4E-binding protein; AMPK, AMP-activated protein kinase; COX, cytochrome *c* oxidase; EB, enteroblast; EC, enterocyte; EE, enteroendocrine; ETC, electron transport chain; FOXO, forkhead box O; ISC, intestinal stem cell; MitoXhoI, mitochondrially targeted *Xho*I endonuclease; mtDNA, mitochondrial DNA; OXPHOS, oxidative phosphorylation; ROS, reactive oxygen species; *ts*, temperature-sensitive lethal; *wt*, wild type.

interspersed among the basal epithelium of the entire adult fly midgut (Buchon, Osman *et al*., 2013; Marianes and Spradling, 2013). ISCs proliferate and give rise to new epithelium in response to tissue injury or stresses (Biteau *et al*., 2011; Jiang and Edgar, 2011; Meng and Biteau, 2015). The ISC usually undergoes an asymmetric division that generates a new ISC and an intermediate progenitor, enteroblast (EB), which can further differentiate into either an absorptive enterocyte (EC) characterized by a polyploid nucleus, or a secretory enteroendocrine (EE) cell at a lower frequency (Ohlstein and Spradling, 2007; Biteau *et al*., 2008; Jiang and Edgar, 2011; Biteau and Jasper, 2014). The simple organization, defined ISC lineage, and ample set of genetic tools available in *Drosophila* make the *Drosophila* midgut an ideal model to explore the impact of ETC complexes on stem cells' activity.

Applying a selection scheme based on a mitochondrially targeted *Xho*I endonuclease (MitoXhoI) (Xu *et al*., 2008), we isolated a temperature-sensitive lethal mtDNA mutation (*ts*), *mt:CoI*^{T300I}, that abolishes the sole *Xho*I site in the cytochrome *c* oxidase (COX) subunit I locus on the *Drosophila* mitochondrial genome (Hill, Chen, and Xu, 2014; Chen *et al*., 2015). The resulting threonine-to-isoleucine substitution destabilizes the association between the mutated CoI protein with the cytochrome A heme, which leads to severely reduced COX activity at the restrictive temperature of 29°C (Chen *et al*., 2015). In tissues or cells harboring a homoplasmic *ts* allele, mitochondrial inner membrane potential is reduced, but there is no accumulation of reactive oxygen species (ROS) (Chen *et al*., 2015). Homoplasmic *ts* flies develop normally at 18°C, but fail to eclose at 29°C. In heteroplasmic flies carrying both the *ts* mtDNA and wild-type (*wt*) mtDNA, tissue-specific expression of MitoXhoI can effectively remove the wild-type mtDNA and results in *ts* homoplasmy in those tissues (Chen *et al*., 2015). In this study, we expressed MitoXhoI in the midgut using the *esg*^{ts} *Flp-Out (esg*^{ts}*F/O)* method (Jiang *et al*., 2009). This genetic scheme generated *ts* homoplasmy in the ISCs and their derivatives in heteroplasmic flies and allowed us to investigate how ETC deficiency impacts ISC's activity in an overall healthy background. We report that deficiencies in cytochrome chain complexes in midgut stem cells impaired their proliferation and blocked the EC specification, which is partially due to an increase of the activity of the FOXO transcription factor.

RESULTS

COX deficiency in *Drosophila* ISCs decreases the number of their differentiated progeny

To study how defective respiration might affect the behavior of *Drosophila* ISCs, we generated clones of ISCs harboring the temperature-sensitive lethal mtDNA mutation (*ts*): *mt:CoI*^{T300I} (Supplemental Figure S1). In heteroplasmic *ts* flies, we drove the expression of a mitochondrially targeted *Xho*I restriction enzyme (*UAS-mitoXhoI*) specifically in ISCs, using the *esg*^{ts}*F/O* system (*esg-GAL4, tub-GAL80*^{ts}*, UAS-nlsGFP/CyO; UAS-flp, act>CD2>GAL4/TM6*) (Jiang *et al*., 2009), to render the ISCs homoplasmic for the *ts* mutation (Chen *et al*., 2015). In this system, GAL4 is specifically expressed in ISCs under the *esg* promoter, but its activity is hampered by ubiquitous GAL80^{ts} at 18°C. Newly emerged adult flies are subjected to a pulse of heat shock at 37°C and maintained at 29°C afterward. This treatment inactivates the GAL80^{ts} protein and allows *esg-Gal4* to activate Flp expression in ISCs (Jiang *et al*., 2009). Flp in turn induces *act>Gal4,* which actives UAS transgenes in all progeny derived from ISCs (Jiang *et al*., 2009). This pulse of heat shock also stresses the midgut to induce ISC proliferation (Strand and Micchelli, 2011). Expression of MitoXhoI removes the wild-type mtDNA in heteroplasmic cells, rendering them homoplasmic for *ts* and deficient in COX activity (Chen *et al*., 2015). Meanwhile, defective cells are labeled with GFP and therefore readily distinguished from healthy cells. As a control, we introduced the same combination of nuclear transgenes in a homoplasmic background harboring an synonymous mtDNA mutation that abolishes the *Xho*I site on *mt:CoI* locus, but does not change the COX amino acid sequence (*mt:Col*^{syn}) (Chen *et al*., 2015). From here on out, we refer to the ISCs and their progeny carrying the *ts* allele as mutant and the ISCs and progeny carrying *mt:Col*^{syn} as control.

In control flies, one third of the midgut was occupied by GFP$^+$ cells 3 d after heat shock. The GFP$^+$ area increased in older flies, reaching 40% and 60% at day 10 and day 20, respectively (Figure 1, A and B). In the mutants, the midguts were fragile during dissection and appeared thinner than in controls. Less than 20% of the tissue was GFP$^+$ at day 3 (Figure 1B), and the proportion of GFP$^+$ area remained the same in older mutant flies (Figure 1B). We stained midguts for Delta, Su(H)GBE-LacZ, Pdm1, and Prospero to mark ISCs, EB, EC, and EE cells, respectively (Supplemental Figure S1, A and C). We also considered the location, shape, and nuclear size of cells to determine cell types. The abundance of ISCs was higher in the mutant than in the control (Supplemental Figure S2A). However, the abundance of GFP$^+$ differentiated cells (EBs, ECs, and EEs) was much lower in mutant midguts compared with control (Figure 1, C and D; Supplemental Figure S2A).

COX deficiency impairs ISC proliferation and EB-to-EC specification

Multipotent ISCs proliferate and generate EB cells, which subsequently differentiate into ECs or EE cells. Thus, the paucity of ISC progeny (EB, EC, and EE cells) in mutant midguts could be caused by either impaired ISC proliferation and differentiation or increased cell death. To test these possibilities, we first assessed apoptosis by staining midguts with an antibody against cleaved-caspase 3, to mark apoptotic cells (Xing *et al*., 2015). Overall, very few cells stained positive for cleaved-caspase 3 in either control or mutant midguts (Figure 2, A and B). They mostly located to the anterior part of midguts and had large nuclei, indicating that they were presumably ECs. Of primary significance, the abundance of apoptotic cells was comparable in control and mutant guts (Figure 2, A and B), demonstrating that apoptosis is not increased in mutant midguts, nor should it be considered the cause of the lack of ISC progeny. Additionally, the numbers of GFP$^+$ ISCs were comparable between control and mutant anterior midguts either 8 or 3 d after induction (Supplemental Figure S2B), further substantiating that the lack of ISC progeny in the mutant midgut is not caused by an increase of ISC death.

To address whether COX deficiency impairs cell proliferation, we examined DNA synthesis via EdU incorporation. Many EdU$^+$ cells were observed in control midguts (Figure 2C and Supplemental Figure S2C), and the majority of these cells had large nuclei (Figure 2C), indicating that they are EB or newborn EC undergoing endoreplication (Xiang *et al*., 2017). A small fraction of EdU$^+$ cells had small nuclei, likely the proliferating ISCs. In mutant midguts, the overall numbers of EdU$^+$ cells were much lower than that in controls (Figure 2C and Supplemental Figure S2C). Very few EdU$^+$ cells with small nuclei were detected in mutant midguts (Figure 2, C and D), suggesting that COX deficiency impairs ISCs' division. We barely observed EdU$^+$ cells with large nuclei (Figure 2C and Supplemental Figure S2C), indicating a lack of endoreplication of EB/EC in the mutant midgut.

The lack of endoreplication could be due to either a lack of EB or impaired EB-to-EC specification. To further test whether ETC disruption impairs EC lineage specification, we replaced the *esg-GAL4* used in the *esg*^{ts}*F/O* system with an EB-specific driver,

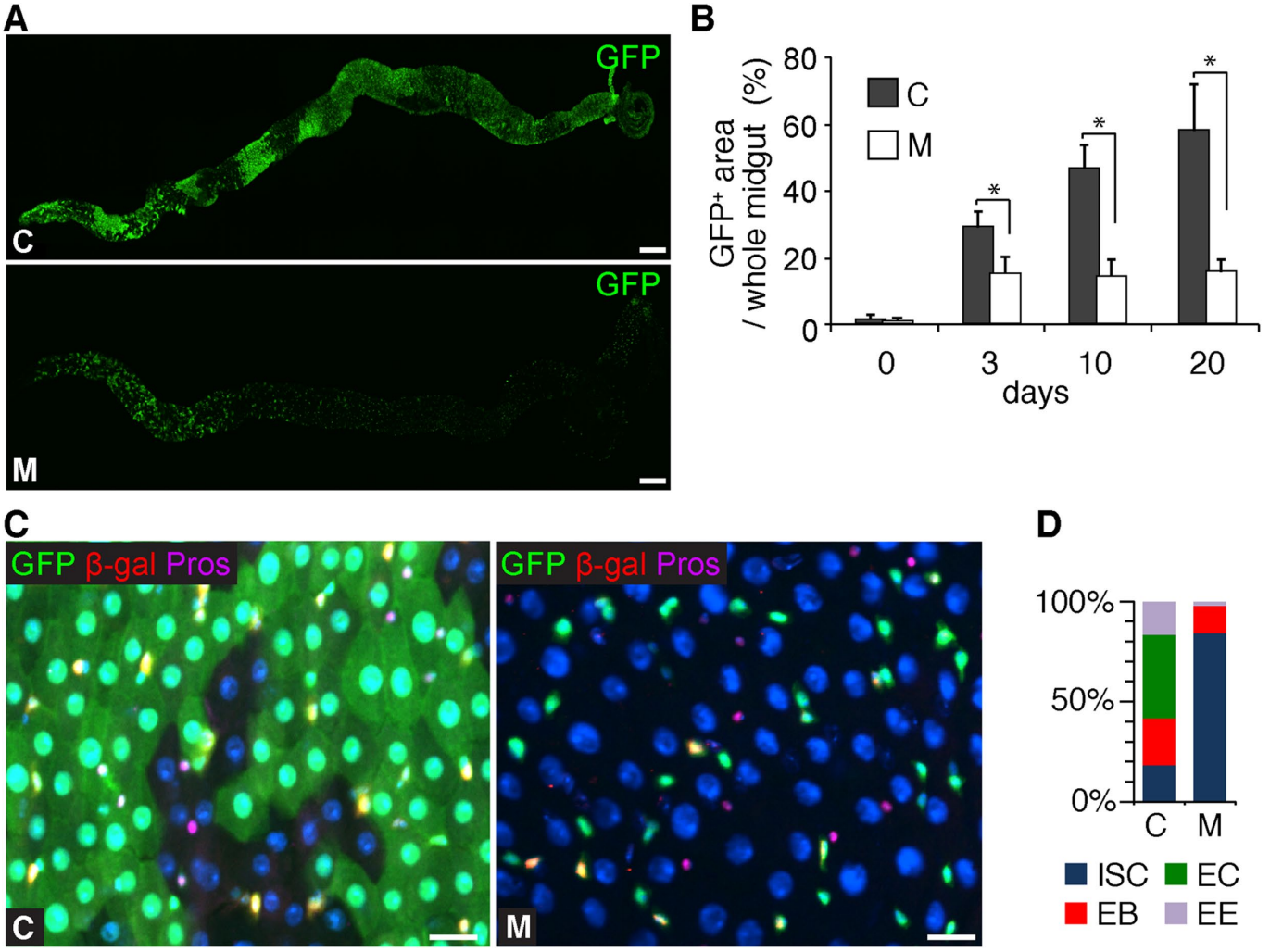

FIGURE 1: There are fewer differentiated cells in midgut carrying a deleterious mtDNA allele. (A) Fewer GFP$^+$ cells in the mutant (M) vs. control (C) midgut (*esg^{ts}F/O>mitoXhoI* flies), 20 d after heat shock. Scale bars: 200 μm. (B) Quantification of the midgut area occupied by GFP$^+$ cells in C and M midguts at different time points after heat shock. $n = 10$ midguts each group, error bar: SD. *: $p < 0.001$. (C) Representative views of the C and M posterior midguts, 10 d after the heat shock, showing significantly fewer GFP$^+$ EB, EC, and EE cells in M than in C midgut. Cell-specific markers are as follows: EB: Su(H)GBE-lacZ (β-gal, red); EC: cell body and nucleus size; and EE: Prospero (magenta). Green: GFP. Scale bars: 10 μm. (D) Bar graph showing the composition of GFP$^+$ cell types in the C and M midguts, 20 d after the heat shock. $n = 10$ midguts each group, C: 3545 cells, M: 1711 cells.

Su(H)GBE-GAL4, to initiate the expression of Flp, GFP, and MitoXhoI in EBs (Figure 3A). We also used the mtDNA synonymous mutation, *mt:Col^{syn}*, as control. Similar to results in the *esg^{ts}F/O* system, the numbers of GFP$^+$ EC were significantly lower in mutant compared with control midguts (Figure 3, B and C), demonstrating that COX deficiency indeed impairs EB-to-EC specification.

ETC deficiencies block ISC proliferation

We initially thought that the *ts* mtDNA would undergo compensatory replication to restore the mtDNA content to normal after the elimination of the wild-type mtDNA in heteroplasmic ISCs (Supplemental Figure S1B). However, mtDNA content in mutant ISCs remained lower than that in control cells (Supplemental Figure S3A), suggesting an incomplete compensatory replication of mtDNA. Thus, aside from defective Complex IV caused by the *ts* mutation, mutant ISCs might also possess inadequate complexes I, III, or V because of reduced mtDNA content. To determine whether the lack of ISC proliferation is specifically pertained to defective Complex IV, we disrupted every single complex independently by knocking down the nuclear encoded components (Figure 4A). We used RNA interference (RNAi) lines that were proven effective in a previous study (Teixeira, Sanchez, Hurd, *et al.*, 2015) and activated them in ISCs and progeny specifically using the *esg^{ts}F/O* system. While disruption of each individual ETC complex impaired ISC proliferation to some extent (Figure 4B; Supplemental Figure S3, B–D), RNAi against genes in complexes III and IV caused much stronger defects than other complexes (Figure 4B; Supplemental Figure S3, B–D).

Active ETC complexes establish mitochondrial inner membrane potential ($\Delta\psi_m$) that drives ATP synthesis. To understand the biochemical deficiency in mutant ISCs, we assessed the $\Delta\psi_m$ using ratiometric imaging between TMRM and MitoTracker-deep red, two fluorescent dyes reporting $\Delta\psi_m$ and mitochondrial mass, respectively. Consistent with previous studies (Chen *et al.*, 2015; Zhang *et al.*, 2019), $\Delta\psi_m$, indicated as the ratio of TMRM to MitoTracker, was markedly reduced in mutant ISCs compared with the control (Supplemental Figure S4, A and B). Depolarized mitochondria are less

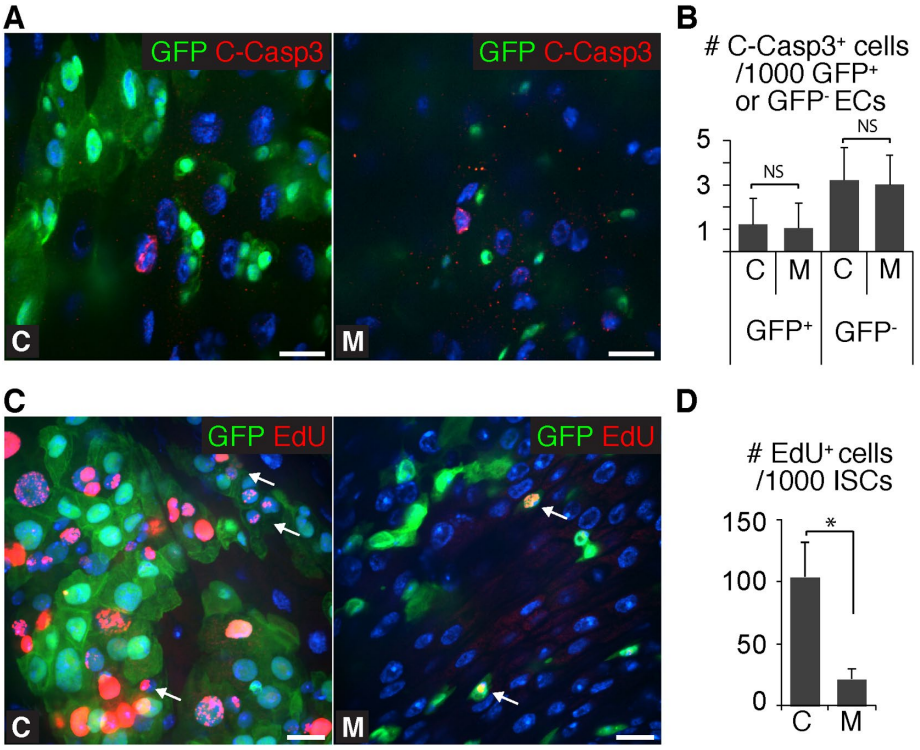

FIGURE 2: COX deficiency impairs ISC proliferation and EB/EC endoreplication but does not trigger ISC apoptosis. (A) Cleaved caspase-3 staining showing equally rare apoptotic cells in both control (C) and mutant (M) midguts (*esg^{ts}F/O>mitoXhoI* flies) 20 d after the heat shock. Green: GFP; Red: cleaved caspase-3; Blue: DAPI. Scale bars: 10 μm. (B) Quantification of the apoptotic cells marked by cleaved caspase-3 staining in C and M midguts, 20 d after the heat shock. $n = 10$ midguts each group; error bar: SD; NS: not significant. (C) EdU incorporation (red) in C and M midguts, 20 d after the heat shock. Nuclear EdU incorporation was detectable in GFP$^+$ cells with either a large or a small nucleus (arrow) in the C midgut, but only in few small-nucleus GFP$^+$ cells in the M midgut. Green: GFP; Red: EdU; Blue: DAPI. Scale bars: 10 μm. (D) Quantification of the EdU$^+$ ISCs in C and M midguts, 20 d after the heat shock. $n = 10$ midguts each group, 1000 ISCs assessed per midgut; error bar: SD; *: $p < 0.001$.

competent in producing ATP compared with energized mitochondria with higher $\Delta\psi_m$. Indeed, midguts carrying the homoplasmic *ts* allele had lower ATP levels compared with control (Supplemental Figure S5A). ATP deficiency, specifically the reduced ATP-to-AMP, ratio can activate AMP-activated protein kinase (AMPK), which inhibits cell proliferation through a P53-dependent pathway in a *Drosophila tenured* mutant affecting the *coxVa* locus on the nuclear genome (Mandal, Guptan, *et al.*, 2005). However, knocking down AMPK failed to rescue the ISC proliferation phenotype in mutant midguts (Supplemental Figure S5, B and C), suggesting that either the reduced supply of ATP, a common consequence of ETC disruption, is not the main cause of the ISC lineage impairments or ATP deficiency may impair ISC activity via a process independent of AMPK.

ETC deficiency blocks the ISC-to-EC specification through FOXO

Electron flow from Complex III to Complex IV is a major step generating ROS (Starkov, 2008; Bleier and Drose, 2013). A previous study demonstrated that ROS can block the cell cycle progression via a FOXO-dependent inhibition on cyclin E/CDK2 (Owusu-Ansah *et al.*, 2008). FOXO is also believed to play important roles in regulating stem cell quiescence and survival (Cheung and Rando, 2013). These observations spurred us to test whether the ROS-FOXO pathway was involved in inhibiting ISC proliferation in mutant midguts.

We first assessed ROS levels by staining midguts with CellROX (Sekihara *et al.*, 2016; Manent *et al.*, 2017), a fluorescent indicator for ROS. CellROX intensity markedly increased in guts pretreated with an organic peroxide, *tert*-butyl hydroperoxide, but was reduced in guts pretreated with a reducing agent, N-acetylcystine (Supplemental Figure S6, A and B), suggesting that CellROX indeed properly indicates the level of ROS. We found that intensities of CellROX were comparable between control and mutant midguts (Supplemental Figure S6, A and B). Additionally, co-overexpression of the ROS-scavenging enzymes SOD2 and catalase (Sun *et al.*, 2002) did not rescue the ISC proliferation in the *ts* mutant background (Supplemental Figure S6, C and D). These results indicate that ROS is not elevated in mutant cells, nor involved in the inhibition of ISC proliferation. By contrast, FOXO protein was markedly increased in ISCs and EBs in the mutant midgut compared with control (Figure 5A) and when Complex III was disrupted (Figure 4A). To assess FOXO activity, we used a *lacZ* reporter under the control of the promoter of the 4E-binding protein (4EBP) gene, a target of FOXO (Puig *et al.*, 2003; Demontis and Perrimon, 2010). We found that the amount of lacZ protein was markedly higher in mutant cells than in controls (Supplemental Figure S7). Taken together, these results demonstrate that FOXO protein and its transcriptional activity are elevated in mutant cells, in the absence of any detectable increase in cellular ROS.

To understand the consequence of FOXO accumulation, we overexpressed FOXO using the *esg^{ts}F/O* system in control midguts and found that it significantly reduced the GFP$^+$ area (Figure 5B and Supplemental Figure S8), indicating that increased FOXO activity can indeed block ISC lineage specification. Reciprocally, knocking down *foxo* in ISCs markedly increased the GFP$^+$ area in mutant midguts (Figure 5, B and C; Supplemental Figure S8). Further classification of cell types demonstrated that *foxo* knockdown in ISCs significantly restored production of GFP$^+$ EB and GFP$^+$ EC but not GFP$^+$ EE cells (Figure 5, C and D). We also carried out RNAi against *foxo* in EBs using the *Su(H)GBE^{ts}F/O* system and found that it restored the number of ECs in the mutant midgut (Supplemental Figure S9). Altogether, these results indicate that FOXO protein is elevated in mutant midguts, blocking the ISC commitment to EB and EB-to-EC specification.

Thor mediates the impairment in EC specification in mutant midguts

To understand how FOXO interferes with ISC's activity, we performed RNA sequencing (RNAseq) on control and mutant ISCs. About 10% of the mRNAs we detected were either up-regulated or down-regulated in the mutant ISCs relative to control (Supplemental

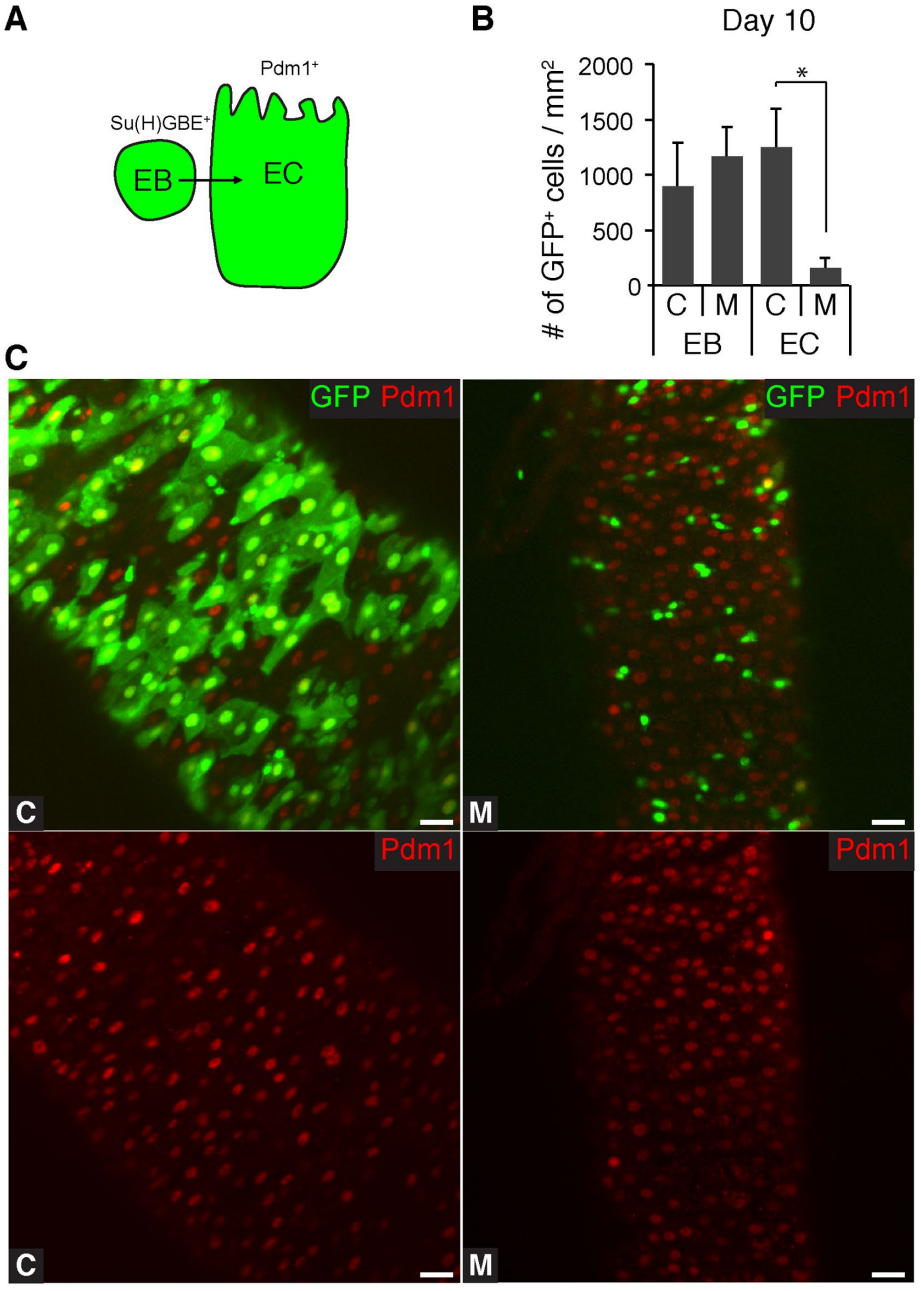

FIGURE 3: COX deficiency blocks EB-to-EC differentiation. (A) Scheme of labeling EB and its progeny using the *Su(H)GBE^{ts}F/O* system. After heat shock, all *Su(H)GBE*$^+$ EB cells and their progeny express GFP and become homoplasmic for either the *ts* allele (M) or *syn* mutation (C). (B) Quantification of the GFP$^+$ EBs and GFP$^+$ ECs in the C and M midguts (*Su(H)GBE^{ts}F/O >mitoXhoI flies*), 10 d after the heat shock. $n = 10$ midguts each group; error bar: SD; *: $p < 0.001$. (C) Representative views of the posterior C and M midguts (*Su(H)GBE^{ts}F/O>mitoXhoI flies*), 10 d after heat shock. Note the significantly fewer GFP$^+$ ECs (Pdm1$^+$ with polyploid nucleus) in M compared with C. Green: GFP; Red: Pdm1. Scale bars: 10 μm.

Table S1). The down-regulated pool included many genes involved in cell differentiation, proliferation, and growth regulation (Supplemental Table S2). The up-regulated pool included genes participating in various metabolic processes (Supplemental Table S2). This result suggests a possible metabolic adaptation in response to the OXPHOS deficiency in mutant midguts. Importantly, knockdown of *foxo* in mutant ISCs restored the expression level of more than 50% of the up- or down- regulated genes (Figure 6A and Supplemental Table S2), indicating that the transcriptional response to COX deficiency is partially mediated by FOXO.

Thor, the sole homologue of *4EBP* in the *Drosophila* genome, was among the genes whose expression was up-regulated in mutant midguts and restored by *foxo* knockdown (Supplemental Table S1). This finding is consistent with previous studies showing that *Thor* is a downstream target of FOXO in the regulation of cell growth and metabolism (Miron *et al.*, 2001; Teleman *et al.*, 2005). 4EBP proteins are highly conserved in metazoans, where they block the initiation of cap-dependent mRNA translation by binding to elongation factor eIF4E (Hernandez *et al.*, 2010; Peter *et al.*, 2015). The transition from EB to EC demands large amount of protein synthesis to drive cell growth, which could explain how the up-regulation of Thor blocks EC specification in mutant midguts. To test this idea, we knocked down *Thor* using *esg^{ts}F/O*-driven RNAi. We found that the number of GFP$^+$ ECs was partially restored (Figure 6, B and C), confirming that the blockage of EC specification is partially mediated by Thor. Additionally, activating the mTOR pathway that inhibits 4EBP, via *Tsc2* knockdown (Kapuria *et al.*, 2012), also led to significantly enlarged GFP positive cells in mutant midguts (Figure 6, D and E), indicating a partial rescue of the EC specification.

So far, our data indicate that ETC deficiencies elevate the FOXO protein level, which blocks EC specification through the 4EBP homologue Thor. However, *foxo* knockdown only restored the expression of a subset of genes altered in the mutant ISCs (Figure 6A and Supplemental Table S2). Additionally, neither *foxo* nor *thor* knockdown restored the number of GFP$^+$ EE cells in mutant midguts (Figures 5D and 6C). These observations suggest that pathways other than *foxo* are likely to be involved in regulating EE specification.

DISCUSSION

Pharmacological disruptions of ETC complexes in cultured embryonic stem cells impair their proliferation and differentiation (Chung *et al.*, 2007; Mandal *et al.*, 2011). However, how mitochondria exert these regulations is still enigmatic. Besides the fact that these studies were carried out in vitro and were complicated by potential side effects of drugs, little evidence has been provided to clarify the role of mitochondrial respiration in regulating stem cell activity in vivo, especially for somatic stem cells that are necessary to maintain tissue homeostasis during aging. To address this question, we genetically disrupted ETC in *Drosophila* intestine stem cells by manipulating their mitochondrial genomes while keeping the environmental

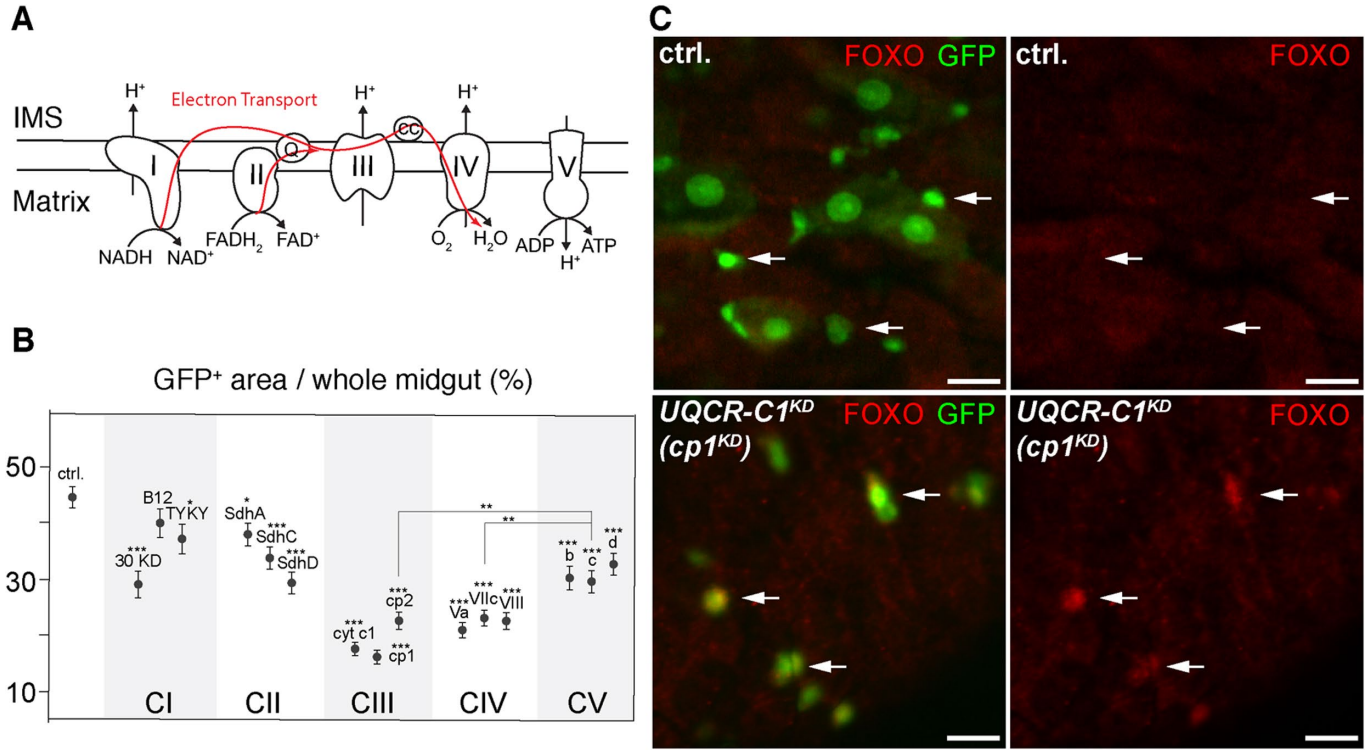

FIGURE 4: The intact ETC is required for ISC proliferation. (A) Schematic representation of electron transportation complexes. (B) Quantification of the midgut area occupied by GFP+ cells in control and gene knockdown *esg^{ts}F/O* flies for nuclear-encoded respiratory complex subunits (Complex I: 30KD [ND30], B12(NDB12), TYKY(ND23); Complex II: SdhA [SdhA], SdhC [SdhC], SdhD [SdhD]; Complex III: cyt c1[cytochrome *c*1], cp1[UQCR-C1], cp2 [UQCR-C2]; Complex IV: Va [COX5A], VIIc [COX7C], VIII [COX8]; Complex V: b [ATPsynB], c [ATPsynC], d]ATPsynD]), 10 d after the heat shock. $n = 10$ midguts each group, error bar: SEM; asterisks above the subunit name indicate the significance compared with RNAi control (*esg^{ts}F/O>luciferase ^{KD}*). *: $p < 0.05$, **: $p < 0.01$, ***: $p < 0.001$. (C) FOXO antibody staining of the control and *UQCR-C1^{KD} esg^{ts}F/O* midguts, 10 d after the heat shock. FOXO protein levels markedly increased in the *UQCR-C1^{KD}* ISCs/EBs (arrows) compared with control. Green: GFP; Red: FOXO; Scale bars: 10 μm.

epithelial niche intact. We found that ETC deficiencies impaired ISC's proliferation and lineage specification.

The defects could be a common consequence of ETC disruption, as similar phenotypes were observed among genetic disruption of different complexes, although the penetrance varied (Figure 4B; Supplemental Figure S3, B–D). Disruption of complexes I and II had a mild effect on ISC proliferation and lineage specification, whereas disruption of complexes III or IV resulted in much stronger defects (Figure 4B; Supplemental Figure S3, B–D), similar to that in ISCs carrying the *ts* allele. Mitochondrial respiration begins with the oxidation of either NADH or succinate by NADH dehydrogenase (Complex I) and succinate dehydrogenase (Complex II) ,respectively (Figure 4A). The partial redundancy between complexes I and II may explain mild phenotypes in RNAi against these two complexes. The most obvious consequence of ETC disruption is ATP deficiency. Although AMPK, the classical energy sensor, is not involved in the manifestation of the ISC phenotype (Supplemental Figure S5, B and C), we cannot rule out the possibility that ATP deficiency might inhibit ISC proliferation through other unnoted processes independent of AMPK. Alternatively, the ISC phenotype may specifically pertain to inhibition of the cytochrome chain in complexes III and IV.

The leakage of free electrons from the cytochrome chain to oxygen is a main source of cellular ROS (Starkov, 2008; Bleier and Drose, 2013). However, in our system, disruption of ETC did not lead to ROS accumulation (Supplemental Figure S6, A and B). Additionally, overexpression of ROS scavengers did not rescue the mutant phenotype (Supplemental Figure S6, C and D), further supporting that ROS accumulation is not the cause of the ISC proliferation defect. Nonetheless, in mutant ISCs, we found elevated expression of FOXO, (Figure 5A), a transcription factor known to be up-regulated in response to ROS stress and to mediate stem cell behavior (Cheung and Rando, 2013; Klotz *et al.*, 2015). Importantly, we found that the elevated FOXO activity is partially responsible for the mutant defect. Hyperactivation of FOXO and elevated FOXO levels have been documented in human disease accompanied by mitochondrial dysfunction and increased oxidative stress (Kannike *et al.*, 2014). The increased FOXO protein levels in these contexts result from FOXO autoregulation via a positive feedback loop. Such a positive autofeedback loop is also reported in the *Drosophila* adult gut (Alic *et al.*, 2014) and may remain active in the mutant ISCs. How ETC disruption leads to elevated FOXO activity in our system is currently unclear. Aside from ROS, the mitochondrial unfolded protein response (UPR^{mt}) causes lasting FOXO activation during *Drosophila* development (Borch Jensen *et al.*, 2017). Could the reduced availability of mtDNA-encoded subunits in mutant ISCs result in UPR^{mt} and eventually activate FOXO? In this case, ETC deficiencies may impact ISC activity indirectly. Recent studies have suggested that some ETC complexes may have other functions besides respiration (Teixeira, Sanchez, Hurd, *et al.*, 2015; Meng, Yamashita, *et al.*, 2017). The possibility of a specific impact of complexes III and IV on FOXO can therefore not be eliminated, though the exact mechanisms remain obscure at this point.

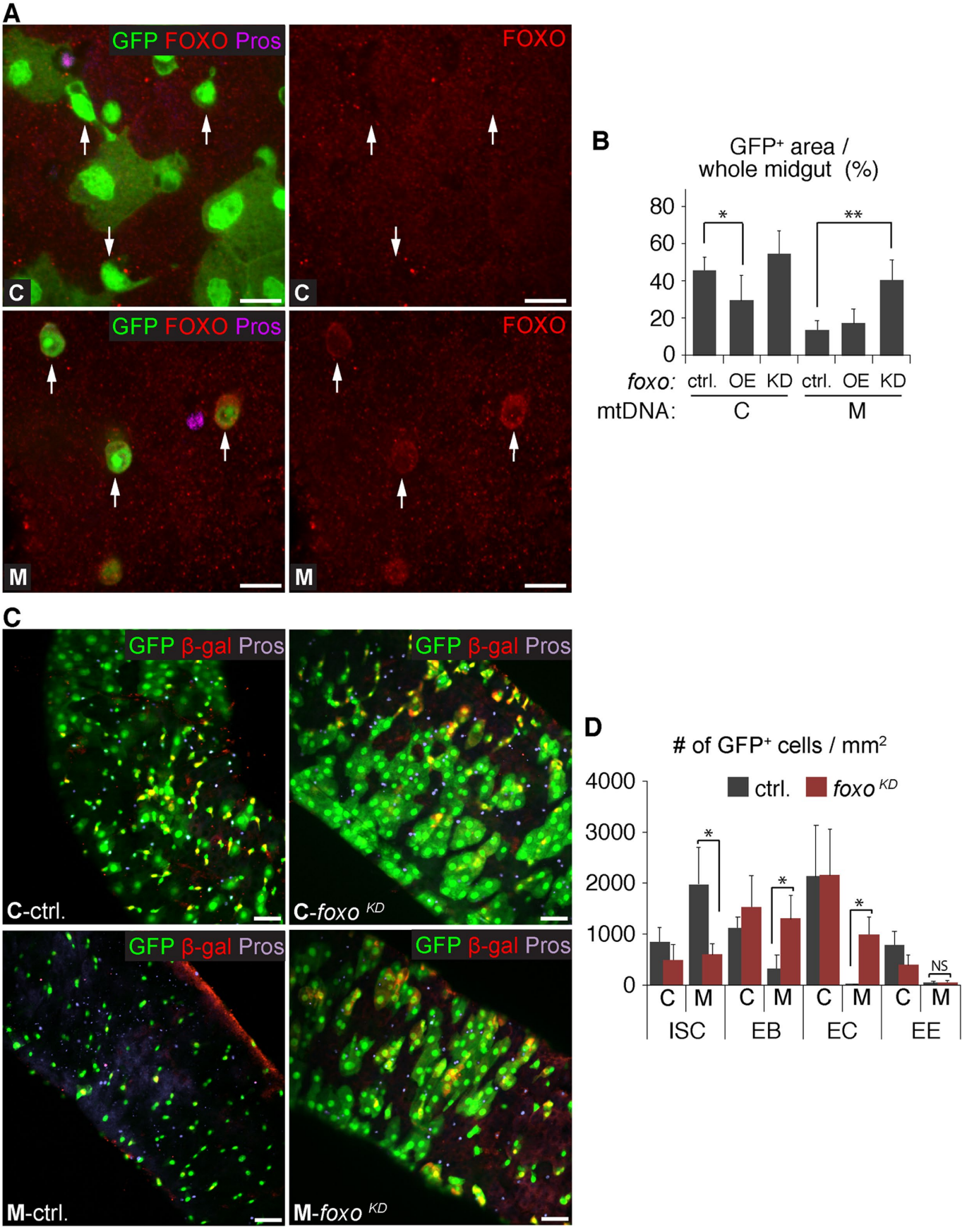
A
GFP FOXO Pros
FOXO
C
C
GFP FOXO Pros
FOXO
M
M
B
GFP+ area / whole midgut (%)
80
60
40
20
0
*
**
foxo: ctrl. OE KD ctrl. OE KD
mtDNA: C M
C
GFP β-gal Pros
GFP β-gal Pros
C-ctrl.
C-foxo KD
GFP β-gal Pros
GFP β-gal Pros
M-ctrl.
M-foxo KD
D
# of GFP+ cells / mm2
ctrl.
foxo KD
4000
3000
2000
1000
0
*
*
*
NS
C M C M C M C M
ISC EB EC EE

As for the impact of elevated FOXO on the ISC lineage, several scenarios are possible. *Drosophila* FOXO functions as a key negative regulator of growth and proliferation, probably via 4EBP transcription (Puig *et al.*, 2003). Indeed, we found that overexpression of FOXO in normal ISCs blocked their lineage specification (Figure 5B and Supplemental Figure S8) and inhibition of FOXO in mutant ISCs partially rescued the defect (Figure 5, C and D), as did down-regulation of 4EBP (Figure 6, B and C). Considering the large size of EC cells that demand prodigious protein synthesis, it is not far-fetched to propose that activation of the FOXO-4EBP cascade could inhibit the formation of EC cells through its inhibition on protein translation and cell growth. Additional support for this notion stems from our observation that activating mTOR, a protein kinase that inactivates 4EBP (Kapuria *et al.*, 2012), led to significantly enlarged GFP-positive cells in mutant midguts, indicating a partial rescue of the EC defect (Figure 6, D and E). Thus, we conclude that FOXO acts at least in part by blocking the cell growth through 4EBP. Besides cell growth, FOXO also regulates metabolism (Nirala, Rahman, *et al.*, 2013), and its upregulation in the *ts* mutant may cause a shift in the ISCs' metabolism. Consistent with this hypothesis, Lactate dehydrogenase that converts pyruvate to lactate and thus shifts the energy metabolism away from OXPHOS (Wang *et al.*, 2016) was significantly up-regulated in mutant ISCs, but restored to normal levels by *foxo* knockdown (Supplemental Table S1). These results suggest that OXPHOS disruption in ISCs caused a metabolic shift that was partially contributed by elevated FOXO, and further support our finding that the intact ETC and aerobic metabolism are essential for ISCs' activity and midgut epithelial homeostasis.

MATERIALS AND METHODS

Fly stocks and transgenic lines

Fly strains used in this study including the following: *w;esg-GAL4,tub-GAL80^{TS},UAS-nlsGFP/CyO;UAS-flp,Act>CD2>GAL4/TM6B* (Jiang *et al.*, 2009); *Su(H)GBE-GAL4, UAS-nlsGFP, tub-GAL80^{TS}* (Zhai *et al.*, 2015); *Su(H)GBE-LacZ* (Micchelli and Perrimon, 2006); *If/CyO;UAS-mitoXhoI*; *UAS-mitoXhoI /CyO;MRKS/TM6B; UAS-SOD2, Catalase; AMPKα* RNAi (BDSC#25931); *foxo* RNAi (BDSC #27656); *UAS-FOXO* (BDSC #42221); *ND30* (30kD) RNAi (VDRC #103412); *NDB12* (B12) RNAi (VDRC #104890); *ND23 (TYKY)* RNAi (VDRC #21748); *SdhA* RNAi (VDRC #110440); *SdhC* RNAi (VDRC #6031); *SdhD* RNAi (VDRC #101739); *Cytochrome c1(cyt c1)* RNAi (VDRC #109809); *UQCR-C1(cp1)* RNAi (VDRC #101350); *UQCR-C2(cp2)* RNAi (VDRC #100818); *COX5A(Va)* RNAi (VDRC #109070); *COX7C(VIIc)* RNAi (VDRC #104970); *COX8(VIII)* RNAi (VDRC #104047); *ATPsynB (b)* RNAi (VDRC #106758); *ATPsynC (c)* RNAi (VDRC #106834); *ATPsynD (d)* RNAi (VDRC #104353); *Thor-lacZ* (4EBP-lacZ, BDSC #9558); *Thor* RNAi (BDSC #36815); *Tsc2* RNAi (BDSC #35401); *UAS-pAbp* (BDSC #9420, for tissue-specific mRNA tagging [Yang *et al.*, 2005]); and *Luciferase* RNAi (BDSC #31603, control for RNAi lines). Female flies of heteroplasmic *mt:Col^{T300I}* and homoplasmic *mt:Col^{syn}* background as previously described (Xu *et al.*, 2008; Chen *et al.*, 2015) were used to generate the mutant (M) group and control (C) group flies for assessments, respectively. All flies and crosses were maintained at 18°C.

Tissue preparation, immunofluorescence staining, and confocal imaging

All fly crosses and the offspring were kept at 18°C. Two days after eclosion, the adult flies for assay were heat-shocked at 37°C for 2 h and maintained at 29°C until dissection at different day points. The entire midgut tissues were dissected out in room temperature Schneider's medium (Thermo Fisher Scientific) supplied with 10% heat inactivated fetal bovine serum (FBS; Thermo Fisher Scientific). The midguts were then rinsed by the same medium and used for either direct imaging or further fixation and staining.

Immunofluorescence staining was done after tissue fixation in phosphate-buffered saline (PBS) containing 4% Paraformaldehyde (PFA) and three times PBS washing. The antibodies and reagents used for staining were mouse anti-Prospero (MR1A; Developmental Studies Hybridoma Bank [DSHB]); mouse anti-delta (C594.9B; DSHB); chicken anti-beta galactosidase (ab9361; Abcam); rabbit anti-Pdm1 (gift from Yu Cai, Temasek Life Sciences Laboratory, National University of Singapore); rabbit anti-cleaved caspase-3 (9661; Cell Signaling); rabbit anti-FOXO antibody (ab195977; Abcam); GFP tag polyclonal antibody, Alexa Fluor 488; Alexa Fluor secondary antibodies (Thermo Fisher Scientific), and Vectashield mounting medium with 4′,6-diamidino-2-phenylindole (DAPI) (Vector Laboratories).

Imaging analysis was performed using the Carl Zeiss Axio Observer equipped with the Perkin Elmer spinning disk confocal system. For live imaging, a Zeiss incubation system was used to maintain proper temperature and humidity. The image processing and quantification were performed by Volocity 6.1.1 software (Perkin Elmer) and ImageJ software (National Institutes of Health [NIH]). Ten midguts were analyzed in each group. The region of the posterior midgut, about 500 μm from the junction of the midgut and hindgut, was used for the quantification of GFP$^+$ cell numbers.

Detection of mitochondrial membrane potential

Mitochondrial membrane potential was detected using a protocol adopted from a previous study (Zhang *et al.*, 2019). Briefly, after dissection, intact guts were incubated in Schneider's medium containing TMRM (200 nM; Thermo Fisher Scientific) and MitoTracker Deep Red (200 nM; Thermo Fisher Scientific) at 29°C for 20 min and rinsed with medium three times. Samples from different groups were mounted with medium on the same coverslip set in a custom-made metal frame and then covered with a small piece of Saran Wrap before imaging. Images were captured with fixed

FIGURE 5: ETC disruption blocks EC specification through FOXO. (A) FOXO antibody staining of the control (C) and mutant (M) midguts (*esg^{ts}F/O>mitoXhoI* flies), 10 d after the heat shock. FOXO protein levels markedly increased in M compared with C ISCs/EBs (arrows). Green: GFP; Red: FOXO; Magenta: Prospero; Blue: DAPI. Scale bars: 10 μm. (B) Quantification shows that *foxo* overexpression (OE) in ISCs significantly reduced the GFP$^+$ midgut area in the C group, 10 d after the heat shock, while *foxo* knockdown (KD) significantly increased the GFP$^+$ area in the M group. $n = 10$ midguts each group, error bar: SD; *: $p < 0.01$, **: $p < 0.001$. (C) Views of the posterior parts of C and M midguts expressing a *foxo* knockdown construct (*esg^{ts}F/O>mitoXhoI*, *foxo ^{KD}* flies) or the RNAi control (*esg^{ts}F/O>mitoXhoI*, *luciferase^{KD}* flies) 20 d after the heat shock. (D) Quantification of C and M GFP$^+$ midgut cell types in the presence or absence of *foxo* knockdown (*foxo^{KD}*). *foxo^{KD}* led to significant increases in the number of GFP$^+$ EBs and GFP$^+$ ECs in M, but not GFP$^+$ EEs. Green: GFP; Red: Su(H)GBE-lacZ (β-gal); Purple: Prospero. Scale bars: 20 μm. $n = 10$ midguts each group, error bar: SD; *: $p < 0.001$, NS: not significant.

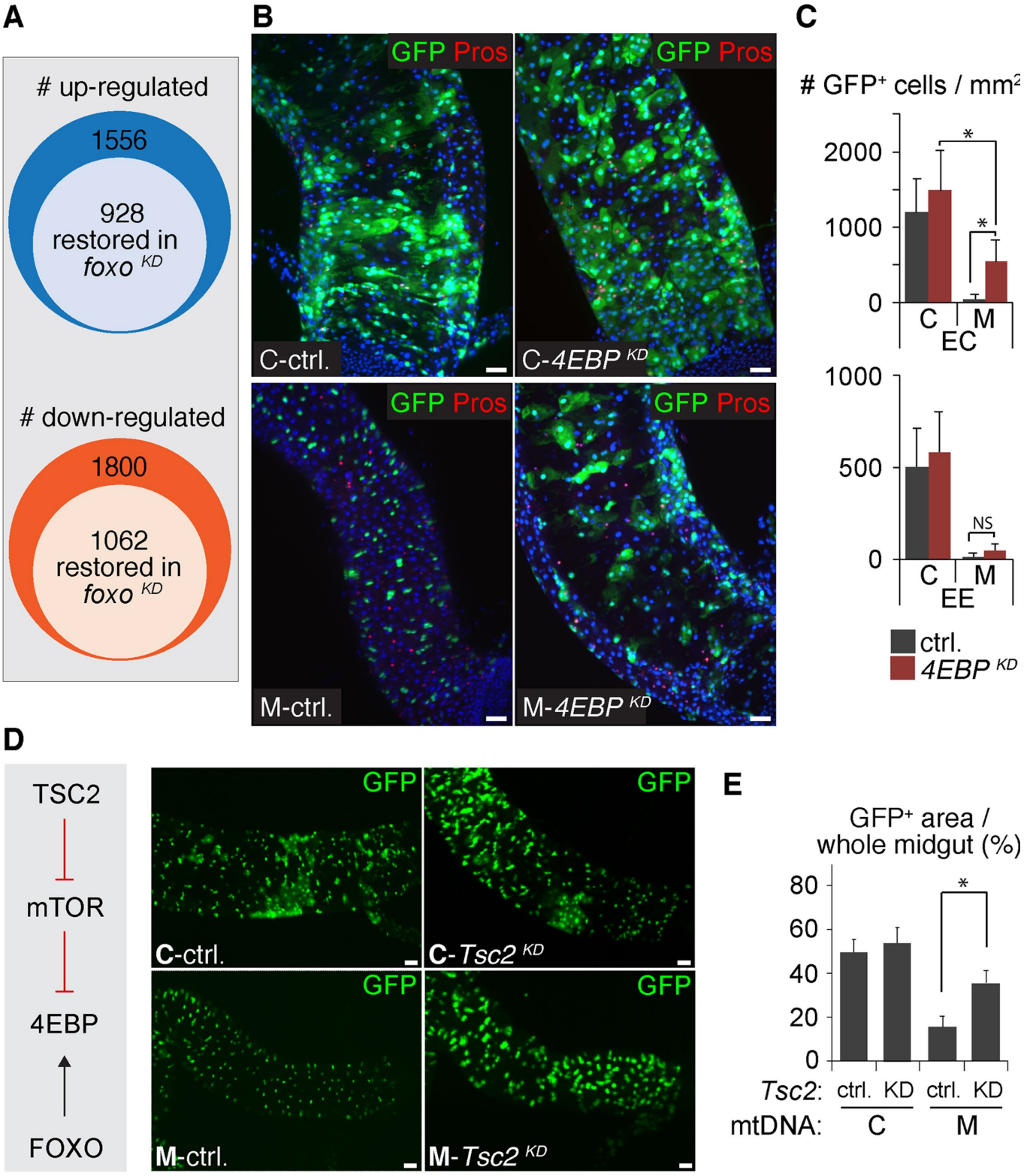

FIGURE 6: The impaired EC specification is partially mediated by 4EBP in mutant midguts. (A) Diagrams summarizing the number of genes up- or down-regulated by ETC disruption and restored by *foxo* knockdown (*foxo*^{KD}). The cut-off was 0.5 CPM (counts per million) fold change averaged across two replicas for regulation by ETC disruption, and 0.25 CPM fold change on average for restoration by *foxo*^{KD}. Full raw data are presented in Supplemental Table S1. (B) Views of posterior midguts expressing a 4EBP knockdown construct (*esg*^{ts}*F/O>mitoXhoI*, *4EBP*^{KD} flies) compared with a control RNAi (*esg*^{ts}*F/O>mitoXhoI*, *luciferase*^{KD} flies) showed partial rescue of GFP$^+$ EC numbers in mutant (M) background. Green: GFP; Red: Prospero; Blue: DAPI. Scale bars: 20 μm. (C) Quantification of the GFP$^+$ ECs and GFP$^+$ EEs in the posterior parts of control (C) and mutant midguts (M) in the presence or absence of *4EBP*^{KD}, 10 d after the heat shock. $n = 10$ midguts each group, error bar: SD; *: $p < 0.001$, NS: not significant. (D) Activation of mTOR pathway

confocal settings. These small, isolated, and basally localized GFP$^+$ cells within the intestinal epithelium were identified as ISCs in esg^{ts} GFP flies based on a previous study (Hochmuth *et al.*, 2011). A single section of basal epithelium was captured, and TMRM and MitoTracker signal intensities were quantified using ImageJ. Mitochondrial membrane potential was computed as the ratio of the mean intensity of TMRM to MitoTracker fluorescence with background correction.

ATP measurement

The tissue ATP level was measured using the ATP Bioluminescence Assay Kit HS II (Roche) following the manufacturer's protocol. Wild-type and homoplasmic *ts* female flies were raised at 18°C for 2 d after eclosion and then shifted to 29°C for 3 d, or continuously maintained at 18°C as control. For each genotype, individual midgut was dissected out and immediately homogenized in 100 µl lysis buffer. The lysates were boiled for 5 min and centrifuged at 20,000 × *g* for 1 min. Cleared lysate (10 µl) was used for ATP measurement using the kit through a 96-well plate luminometer (Berthold). The amount of ATP was then determined and normalized with the protein level measured by BCA protein assay (Thermo Fisher Scientific).

Detection of ROS levels

ROS levels were detected using CellROX Deep Red following the manufacturer's protocol (Thermo Fisher Scientific). Briefly, the guts were incubated in Schneider's medium containing 5 µM CellROX Deep Red for 45 min at 29°C followed by three washes with PBS. The samples were then fixed with 3.7% formaldehyde for 15 min and mounted for imaging analysis. For comparison and quantification, the dissected guts were preincubated in Schneider's medium with or without drugs for 1 h at 29°C before CellROX staining. Control gut incubated in the medium containing 200 µM *tert*-butyl hydroperoxide (TBHP) was used as the positive control, and control gut incubated with 1 mM N-acetylcysteine (NAC) was used as the negative control. Images were captured with a spinning disk confocal system. These small, isolated, and basally localized GFP$^+$ cells within the intestinal epithelium were identified as ISCs in esg^{ts} GFP flies based on a previous study (Hochmuth *et al.*, 2011). A single section of basal epithelium was captured, and CellROX intensity was quantified using Volocity 6.1.1 software (Perkin Elmer).

GFP-positive ISCs sorting and mtDNA level

The GFP$^+$ ISCs were sorted as previously described (Dutta *et al.*, 2013). Briefly, midguts of "*w; esg-GAL4, tub-GAL80^{ts} UAS-nlsGFP/UAS-mitoXhoI*" flies with different mtDNA background, which were heat-shocked and maintained at 29°C for 7 or 15 d, were dissected in PBS and dissociated for 2 h by incubating with 0.8 mg/ml elastase at 29°C. ISCs were then sorted based on intensity of the GFP marker with the help of the Flow Cytometry (FACS) Core Facility of the National Heart, Lung, and Blood Institute (NHLBI), NIH. To quantify the mtDNA level, total DNA was prepared from the sorted samples using the DNeasy Blood kit (Qiagen). Quantitative real-time PCRs were performed in triplicate using the Roche LightCycler 480 system and SYBR Green I Master. Primers based on mtCol (F: ATTGGAGTTAATTTAACATTTTTTCCTCA; R: AGTTGATACAATATTTCATGTTGT- GTAAG) and His4 (F: TCCAAGGTATCACGAAGCC; R: AACCTTCAGAACGCCAC) sequences were used for the mtDNA and nuclear DNA, respectively.

EdU Incorporation

EdU incorporation was determined following a protocol previously described (Zhang *et al.*, 2015), using the Click-iT EdU Alexa Fluor 555 Imaging kit (Thermo Fisher Scientific). Briefly, intact guts were dissected from adult female flies and were incubated in 10 µM EdU in Schneider's medium containing 10% FBS for 2 h at 25°C. Tissues were then fixed with 4% PFA, washed in PBS with 0.1% Triton X-100 (PBST), processed with the kit, and mounted for imaging analysis.

ISC specific mRNA profiling

A modified mRNA tagging technique (Yang *et al.*, 2005) was used to isolate mRNA from ISCs of fly midguts. Briefly, the FLAG-tagged poly(A)-binding protein (pAbp) was expressed in C and M group flies under *esg-GAL4* driver. About 200 midguts from C and M group "*esg-GAL4,tub-GAL80^{TS},UAS-nlsGFP/UAS-mitoXhoI;UAS-pAbp-FLAG/+*" or "*esg-GAL4,tub-GAL80^{TS},UAS-nlsGFP/UAS-mitoXhoI;UAS-pAbp-FLAG/UAS-FOXO-IR*" flies, which were heat-shocked and maintained in 29°C for 5 d, were fixed in 1 ml of PBS containing 1% formaldehyde (Sigma-Aldrich) and 0.5% Igepal CA-630 (Sigma-Aldrich) for 1 h on ice and then incubated for 5 min after the addition of 140 µl of 2 M glycine. Samples were rinsed three times with ice cold PBS and homogenized by sonication in 2 ml of homogenization buffer (150 mM NaCl, 50 mM HEPES buffer at pH 7.6, 1 mM ethylene glycol tetraacetic acid (EGTA), 15 mM EDTA and 10% glycerol) supplied with 8 mM vanadyl ribonucleoside complex (Sigma-Aldrich), 50 U/ml SUPERase-In (Thermo Fisher Scientific), and 1 tablet/50 ml protease inhibitor cocktail tablet (Roche). After centrifugation at 13,000 × *g* for 30 min, the supernatant was incubated with anti-FLAG-M2 affinity agarose beads (Thermo Fisher Scientific) at 4°C overnight (O/N). The beads were then washed four times with homogenization buffer. The RNAs bound to the pAbp were recovered in 100 ml of elution buffer (50 mM Tris-HCl, pH 7.0, 10 mM EDTA, 1.3% SDS, and 50 U/ml SUPERase-In) by proteinase K (40 µg/ml) treatment for 2 h at 60°C and O/N at 65°C after addition of NaCl (200 mM). Eluant was then mixed with 4 vol of Trizol (Thermo Fisher Scientific) and 1 vol of chloroform (Sigma-Aldrich) with vigorous shaking, incubated at room temperature for 10 min, and then centrifuged at 12,000 × *g* for 15 min at 4°C. The supernatant was transferred and mixed with 2.5 vol of isopropanol, chilled at –80°C O/N, and centrifuged at 12,000 × *g* for 30 min at 4°C. The RNA pellet was rinsed twice with 70% ethanol and then dissolved in RNase free water. Poly(A) capture libraries were generated at the DNA Sequencing and Genomics Core, NHLBI, NIH. RNA sequencing was performed with a Hiseq3000 (Illumina), and 75–base pair pair-end reads were generated at the DNA Sequencing and Genomics Core, NHLBI, NIH. RNA sequencing data were analyzed by the Bioinformatics and Computational Biology Core, NHLBI, NIH. After quality control (QC) assessment of FASTQ files using FastQC toolkit (v0.11.5) with default parameters. paired-end reads were aligned against the *Drosophila melanogaster* reference genome

by *Tsc2* knockdown in ISCs showed enlarged GFP$^+$ cells in mutant midguts (*esg^{ts}F/O>mitoXhoI, Tsc2^{KD}* flies), indicating a partial rescue. Assessed 10 d after the heat shock. Scale bars: 20 µm. (E) Quantification shows that *Tsc2* knockdown (KD) in ISCs significantly increased the GFP$^+$ midgut area due to enlarged GFP$^+$ cells in mutant midguts, 10 d after the heat shock. $n = 10$ midguts each group, error bar: SD; *: $p < 0.001$.

(Dmel6) using HISAT2 (v2.0.5) alignment. Gene level read counts were produced by featureCounts (v1.5.2) using paired-end, reversely stranded read. Differential expression analysis at the gene level was carried out using limma-voom open source R packages. TMM normalization was carried out, and normalized factors were estimated for each sample. The lmFit function in limma-voom was used to fit linear models for each gene to calculate log2 fold changes and *p* values using the normalized factors as weights in the model. The cut-off for gene up- or down-regulation in M relative to C was 0.5 CPM fold change averaged across two replicas, and the cut-off for restoration by $foxo^{KD}$ was 0.25 CPM fold change in M- $foxo^{KD}$ relative to C- $foxo^{KD}$.

The RNAseq data were deposited in the Gene Expression Omnibus of the National Center for Biotechnology Information and are available with accession number (GEO: GSE137231, Secure token: onolokmgbrmzlgp) https://www.ncbi.nlm.nih.gov/geo/query/acc.cgi?acc=GSE137231 .

Statistical analysis

The *F* test was performed to evaluate the equality of variances. Two-tailed Student's t test was used for statistical analysis. Difference was considered statistically significant when $p < 0.05$. Results are represented as mean ± SD of the number of determinations.

ACKNOWLEDGMENTS

We thank F. Chanut for comments and editing on the manuscript; B. Edgar, N. Perrimon, Z. Zhai, the Bloomington Drosophila Stock Center, and the Vienna Drosophila Resource Center for various fly lines; Y. Cai and the Developmental Studies Hybridoma Bank for various antibodies; the National Heart, Lung, and Blood Institute (NHLBI) DNA Sequencing and Genomics Core, and the NHLBI FACS core for technical assistance. This work is supported by the NHLBI Intramural Research Program.

REFERENCES

Boldface names denote co–first authors.

Alic N, Giannakou ME, Papatheodorou I, Hoddinott MP, Andrews TD, Bolukbasi E, Partridge L (2014). Interplay of dFOXO and two ETS-family transcription factors determines lifespan in Drosophila melanogaster. PLoS Genet 10, e1004619.

Biteau B, Hochmuth CE, Jasper H (2008). JNK activity in somatic stem cells causes loss of tissue homeostasis in the aging Drosophila gut. Cell Stem Cell 3, 442–455.

Biteau B, Hochmuth CE, Jasper H (2011). Maintaining tissue homeostasis: dynamic control of somatic stem cell activity. Cell Stem Cell 9, 402–411.

Biteau B, Jasper H (2014). Slit/Robo signaling regulates cell fate decisions in the intestinal stem cell lineage of Drosophila. Cell Rep 7, 1867–1875.

Bleier L, Drose S (2013). Superoxide generation by complex III: from mechanistic rationales to functional consequences. Biochim Biophys Acta 1827, 1320–1331.

Borch Jensen M, Qi Y, Riley R, Rabkina L, Jasper H (2017). PGAM5 promotes lasting FoxO activation after developmental mitochondrial stress and extends lifespan in Drosophila. Elife 6, e26952.

Buchon N, Osman D, David FP, Fang HY, Boquete JP, Deplancke B, Lemaitre B (2013). Morphological and molecular characterization of adult midgut compartmentalization in Drosophila. Cell Rep 3, 1725–1738.

Chen Z, Qi Y, French S, Zhang G, Covian Garcia R, Balaban R, Xu H (2015). Genetic mosaic analysis of a deleterious mitochondrial DNA mutation in Drosophila reveals novel aspects of mitochondrial regulation and function. Mol Biol Cell 26, 674–684.

Cherry AB, Gagne KE, McLoughlin EM, Baccei A, Gorman B, Hartung O, Miller JD, Zhang J, Zon RL, Ince TA, *et al.* (2013). Induced pluripotent stem cells with a mitochondrial DNA deletion. Stem Cells 31, 1287–1297.

Cheung TH, Rando TA (2013). Moleular regulation of stem cell quiescence. Nat Rev Mol Cell Biol 14, 329–340.

Cho YM, Kwon S, Pak YK, Seol HW, Choi YM, Park DJ, Park KS, Lee HK (2006). Dynamic changes in mitochondrial biogenesis and antioxidant enzymes during the spontaneous differentiation of human embryonic stem cells. Biochem Biophys Res Commun 348, 1472–1478.

Chung S, Dzeja PP, Faustino RS, Perez-Terzic C, Behfar A, Terzic A (2007). Mitochondrial oxidative metabolism is required for the cardiac differentiation of stem cells. Nat Clin Pract Cardiovasc Med 4 (Suppl 1), S60–S67.

Demontis F, Perrimon N (2010). FOXO/4E-BP signaling in Drosophila muscles regulates organism-wide proteostasis during aging. Cell 143, 813–825.

Diaz-Castro B, Pardal R, Garcia-Flores P, Sobrino V, Duran R, Piruat JI, Lopez-Barneo J (2015). Resistance of glia-like central and peripheral neural stem cells to genetically induced mitochondrial dysfunction-differential effects on neurogenesis. EMBO Rep 16, 1511–1519.

Dutta D, Xiang J, Edgar BA (2013). RNA expression profiling from FACS-isolated cells of the Drosophila intestine. Curr Protoc Stem Cell Biol 27, Unit 2F 2.

Facucho-Oliveira JM, Alderson J, Spikings EC, Egginton S, St John JC (2007). Mitochondrial DNA replication during differentiation of murine embryonic stem cells. J Cell Sci 120, 4025–4034.

Folmes CD, Dzeja PP, Nelson TJ, Terzic A (2012). Metabolic plasticity in stem cell homeostasis and differentiation. Cell Stem Cell 11, 596–606.

Hernandez G, Altmann M, Lasko P (2010). Origins and evolution of the mechanisms regulating translation initiation in eukaryotes. Trends Biochem Sci 35, 63–73.

Hill JH, Chen Z, Xu H (2014). Selective propagation of functional mitochondrial DNA during oogenesis restricts the transmission of a deleterious mitochondrial variant. Nat Genet 46, 389–392.

Hochmuth CE, Biteau B, Bohmann D, Jasper H (2011). Redox regulation by Keap1 and Nrf2 controls intestinal stem cell proliferation in Drosophila. Cell Stem Cell 8, 188–199.

Inoue S, Noda S, Kashima K, Nakada K, Hayashi J, Miyoshi H (2010). Mitochondrial respiration defects modulate differentiation but not proliferation of hematopoietic stem and progenitor cells. FEBS Lett 584, 3402–3409.

Jiang H, Edgar BA (2011). Intestinal stem cells in the adult Drosophila midgut. Exp Cell Res 317, 2780–2788.

Jiang H, Patel PH, Kohlmaier A, Grenley MO, McEwen DG, Edgar BA (2009). Cytokine/Jak/Stat signaling mediates regeneration and homeostasis in the Drosophila midgut. Cell 137, 1343–1355.

Kannike K, Sepp M, Zuccato C, Cattaneo E, Timmusk T (2014). Forkhead transcription factor FOXO3a levels are increased in Huntington disease because of overactivated positive autofeedback loop. J Biol Chem 289, 32845–32857.

Kapuria S, Karpac J, Biteau B, Hwangbo D, Jasper H (2012). Notch-mediated suppression of TSC2 expression regulates cell differentiation in the Drosophila intestinal stem cell lineage. PLoS Genet 8, e1003045.

Klotz LO, Sanchez-Ramos C, Prieto-Arroyo I, Urbanek P, Steinbrenner H, Monsalve M (2015). Redox regulation of FoxO transcription factors. Redox Biol 6, 51–72.

Lisowski P, Kannan P, Mlody B, Prigione A (2018). Mitochondria and the dynamic control of stem cell homeostasis. EMBO Rep 19, e45432.

Mandal S, Guptan P, Owusu-Ansah E, Banerjee U (2005). Mitochondrial regulation of cell cycle progression during development as revealed by the tenured mutation in Drosophila. Dev Cell 9, 843–854.

Mandal S, Lindgren AG, Srivastava AS, Clark AT, Banerjee U (2011). Mitochondrial function controls proliferation and early differentiation potential of embryonic stem cells. Stem Cells 29, 486–495.

Manent J, Banerjee S, de Matos Simoes R, Zoranovic T, Mitsiades C, Penninger JM, Simpson KJ, Humbert PO, Richardson HE (2017). Autophagy suppresses Ras-driven epithelial tumourigenesis by limiting the accumulation of reactive oxygen species. Oncogene 36, 5576–5592.

Marianes A, Spradling AC (2013). Physiological and stem cell compartmentalization within the Drosophila midgut. Elife 2, e00886.

Meng FW, Biteau B (2015). A Sox transcription factor is a critical regulator of adult stem cell proliferation in the Drosophila intestine. Cell Rep 13, 906–914.

Meng H, Yamashita C, Shiba-Fukushima K, Inoshita T, Funayama M, Sato S, Hatta T, Natsume T, Umitsu M, Takagi J, *et al.* (2017). Loss of Parkinson's disease-associated protein CHCHD2 affects mitochondrial crista structure and destabilizes cytochrome c. Nat Commun 8, 15500.

Micchelli CA, Perrimon N (2006). Evidence that stem cells reside in the adult Drosophila midgut epithelium. Nature 439, 475–479.

Miron M, Verdu J, Lachance PE, Birnbaum MJ, Lasko PF, Sonenberg N (2001). The translational inhibitor 4E-BP is an effector of PI(3s)K/Akt signalling and cell growth in Drosophila. Nat Cell Biol 3, 596–601.

Moraes CT (2001). What regulates mitochondrial DNA copy number in animal cells? Trends Genet 17, 199–205.
Nirala NK, Rahman M, Walls SM, Singh A, Zhu LJ, Bamba T, Fukusaki E, Srideshikan SM, Harris GL, Ip YT, *et al*. (2013). Survival response to increased ceramide involves metabolic adaptation through novel regulators of glycolysis and lipolysis. PLoS Genet 9, e1003556.
Ohlstein B, Spradling A (2007). Multipotent Drosophila intestinal stem cells specify daughter cell fates by differential notch signaling. Science 315, 988–992.
Owusu-Ansah E, Yavari A, Mandal S, Banerjee U (2008). Distinct mitochondrial retrograde signals control the G1-S cell cycle checkpoint. Nat Genet 40, 356–361.
Peter D, Igreja C, Weber R, Wohlbold L, Weiler C, Ebertsch L, Weichenrieder O, Izaurralde E (2015). Molecular architecture of 4E-BP translational inhibitors bound to eIF4E. Mol Cell 57, 1074–1087.
Prigione A, Fauler B, Lurz R, Lehrach H, Adjaye J (2010). The senescence-related mitochondrial/oxidative stress pathway is repressed in human induced pluripotent stem cells. Stem Cells 28, 721–733.
Puig O, Marr MT, Ruhf ML, Tjian R (2003). Control of cell number by Drosophila FOXO: downstream and feedback regulation of the insulin receptor pathway. Genes Dev 17, 2006–2020.
Rafalski VA, Mancini E, Brunet A (2012). Energy metabolism and energy-sensing pathways in mammalian embryonic and adult stem cell fate. J Cell Sci 125, 5597–5608.
Sekihara S, Shibata T, Hyakkendani M, Kawabata SI (2016). RNA interference directed against the transglutaminase gene triggers dysbiosis of gut microbiota in Drosophila. J Biol Chem 291, 25077–25087.
Starkov AA (2008). The role of mitochondria in reactive oxygen species metabolism and signaling. Ann NY Acad Sci 1147, 37–52.
Strand M, Micchelli CA (2011). Quiescent gastric stem cells maintain the adult Drosophila stomach. Proc Natl Acad Sci USA 108, 17696–17701.
Sun J, Folk D, Bradley TJ, Tower J (2002). Induced overexpression of mitochondrial Mn-superoxide dismutase extends the life span of adult Drosophila melanogaster. Genetics 161, 661–672.
Teixeira FK, Sanchez CG, Hurd TR, Seifert JR, Czech B, Preall JB, Hannon GJ, Lehmann R (2015). ATP synthase promotes germ cell differentiation independent of oxidative phosphorylation. Nat Cell Biol 17, 689–696.
Teleman AA, Chen YW, Cohen SM (2005). 4E-BP functions as a metabolic brake used under stress conditions but not during normal growth. Genes Dev 19, 1844–1848.
Vander Heiden MG, Cantley LC, Thompson CB (2009). Understanding the Warburg effect: the metabolic requirements of cell proliferation. Science 324, 1029–1033.
von Heimburg D, Hemmrich K, Zachariah S, Staiger H, Pallua N (2005). Oxygen consumption in undifferentiated versus differentiated adipogenic mesenchymal precursor cells. Respir Physiol Neurobiol 146, 107–116.
Wallace DC (2012). Mitochondria and cancer. Nat Rev Cancer 12, 685–698.
Wanet A, Remacle N, Najar M, Sokal E, Arnould T, Najimi M, Renard P (2014). Mitochondrial remodeling in hepatic differentiation and dedifferentiation. Int J Biochem Cell Biol 54, 174–185.
Wang CW, Purkayastha A, Jones KT, Thaker SK, Banerjee U (2016). In vivo genetic dissection of tumor growth and the Warburg effect. Elife 5, e18126.
Xiang J, Bandura J, Zhang P, Jin Y, Reuter H, Edgar BA (2017). EGFR-dependent TOR-independent endocycles support Drosophila gut epithelial regeneration. Nat Commun 8, 15125.
Xing Y, Su TT, Ruohola-Baker H (2015). Tie-mediated signal from apoptotic cells protects stem cells in Drosophila melanogaster. Nat Commun 6, 7058.
Xu H, DeLuca SZ, O'Farrell PH (2008). Manipulating the metazoan mitochondrial genome with targeted restriction enzymes. Science 321, 575–577.
Yang Z, Edenberg HJ, Davis RL (2005). Isolation of mRNA from specific tissues of Drosophila by mRNA tagging. Nucleic Acids Res 33, e148.
Zhai Z, Kondo S, Ha N, Boquete JP, Brunner M, Ueda R, Lemaitre B (2015). Accumulation of differentiating intestinal stem cell progenies drives tumorigenesis. Nat Commun 6, 10219.
Zhang F, Qi Y, Zhou K, Zhang G, Linask K, Xu H (2015). The cAMP phosphodiesterase Prune localizes to the mitochondrial matrix and promotes mtDNA replication by stabilizing TFAM. EMBO Rep 16, 520–527.
Zhang Y, Marsboom G, Toth PT, Rehman J (2013). Mitochondrial respiration regulates adipogenic differentiation of human mesenchymal stem cells. PLoS One 8, e77077.
Zhang Y, Wang ZH, Liu Y, Chen Y, Sun N, Gucek M, Zhang F, Xu H (2019). PINK1 inhibits local protein synthesis to limit transmission of deleterious mitochondrial DNA mutations. Mol Cell 73, 1127–1137.e1125.
Zheng X, Boyer L, Jin M, Mertens J, Kim Y, Ma L, Ma L, Hamm M, Gage FH, Hunter T (2016). Metabolic reprogramming during neuronal differentiation from aerobic glycolysis to neuronal oxidative phosphorylation. Elife 5, e13374.